Solvation Dynamics of Electron Produced by Two-Photon Ionization of Liquid Polyols. II. Propanediols

J. Bonin,[†] I. Lampre, P. Pernot, and M. Mostafavi*

Laboratoire de Chimie Physique/ELYSE, Univ Paris-Sud, UMR 8000, Bât. 349, Orsay, France 91405, and CNRS, Orsay, France 91405

Received: December 4, 2006; In Final Form: March 15, 2007

Temporal evolution of transient absorption spectra of electrons produced by two-photon ionization of two isomers, propane-1,2-diol (12PD) and propane-1,3-diol (13PD), with 263 nm femtosecond laser pulses has been studied on picosecond time scale. The two-photon absorption coefficients of 12PD and 13PD at 263 nm were determined to be $\beta = (2.0 \pm 0.3) \times 10^{-11}$ and $(2.4 \pm 0.3) \times 10^{-11}$ m W^{-1}, respectively. Time-resolved absorption spectra ranging from 440 to 720 nm have been measured, showing a blue shift for the first tens of picoseconds for both solvents. However, the observed solvation dynamics of electron appears faster in 13PD than in 12PD. The transient signals of electron solvation have then been reconstructed with different models (stepwise mechanism or continuous relaxation model) using a Bayesian data analysis method. Results are discussed, compared with those previously obtained in ethylene glycol (*J. Phys. Chem. A* **2006**, *110,* 1705) and corroborate the interpretation, according to which the solvation of electrons is mainly governed by continuous solvent molecular motions.

1. Introduction

Much research has been focused on understanding the mechanisms of thermalization, localization, and solvation of an excess electron in liquid solvents, particularly in water. Due to the development of ultrashort laser pulses, great strides have been made in the observation of the dynamics of this electron on subpicosecond to picosecond time scales.[1−18] The initial work of Migus et al.[1] and subsequent studies in water[3] and alcohols[2,16,18] suggested the existence of infrared absorbing precursors of the solvated electron. However, other works on electron solvation favored a continuous relaxation, often called "continuous shift" model, in which the existence of infrared absorbing species is not required.[13,14,19] Combinations of both mechanisms, stepwise and continuous models, have also been proposed to account for the observed spectral evolution.[5,7,20,21]

As described in our preceding paper, which is referred to henceforth as paper I,[22] this context instigates our study of the ultrafast dynamics of electron in liquid polyols. In paper I, the solvation dynamics of the electron in ethylene glycol (EG, ethane-1,2-diol) have been detailed. The electron was produced by two-photon ionization of the solvent with 263 nm femtosecond laser pulses. The two-photon absorption coefficient of EG at 263 nm was determined to be $\beta = (2.1 \pm 0.2) \times 10^{-11}$ m W^{-1}. Transient absorption spectra were recorded in the visible domain between 430 and 720 nm for the first 50 ps. In that time range, the electron decay due to geminate recombination is negligible. At very short delay time after the pump pulse, the excess electron in EG presents a very broad absorption band in the visible and near-infrared domain with a maximum around 675 nm. The red part of the absorption band drops rapidly for the first 5 ps while the blue part increases slightly, leading to a blue shift of the absorption band maximum down to 590 nm. Then the absorbance on the red side of the spectrum follows its decrease while the absorbance on the blue side remains nearly constant. As a consequence, the maximum of the absorption band continues to shift toward shorter wavelengths and, 50 ps after the pump pulse, is around 570 nm, the position of the absorption band maximum of the equilibrated solvated electron in EG. Using a Bayesian data analysis method to obtain parametric identification and model comparison, we performed a fitting procedure of the spectro-kinetics signals with different models. Sequential stepwise models with two, three and four states or species were tested. It appeared that at least three species are necessary but sufficient to properly adjust the data. We also wondered whether our observations could be explained by continuous relaxation models. We did not postulate that the absorption profile of the electron shifts, as a whole, to the blue during the solvation, without changing its shape. But, we described the time-dependent absorption spectrum by a log-normal function with time-dependent parameters, the amplitude $\epsilon(t)$, the peak position $E_{max}(t)$, the full width at half-maximum $\Omega(t)$ and the asymmetry $\gamma(t)$. The time dependence of each parameter was modeled by a mono-, bi- or triexponential function or by a stretched exponential function. We obtained a very good fit of the data using biexponential functions with the same characteristic times $\tau_1 \cong 1.7$ ps and $\tau_2 \cong 25.5$ ps for the parameters $E_{max}(t)$, $\Omega(t)$, $\gamma(t)$ and a monoexponential function with $\tau \cong 1$ ps for the amplitude $\epsilon(t)$. Stretched exponential functions provided a good adjustment of the signals, too. But, we found small values for the parameters $\beta < 0.5$, corresponding to very broad distributions of exponential relaxation times, which make difficult the physical interpretation of the stretched exponential function. We also tried the "hybrid" model proposed by Pépin et al.[5] in which two initial unrelaxed species, $e^-_{wb,1}$ and $e^-_{sb,2}$, undergo continuous blue shift with spectra keeping the same shapes and the $e^-_{wb,1}$ species converts into $e^-_{sb,2}$ relaxing to the fully solvated electron. That model did not

* Corresponding author. E-mail: mehran.mostafavi@lcp.u-psud.fr.
[†] Present address: Laboratoire d'Electrochimie Moléculaire, Universté Paris 7 Denis Diderot, 2 Place Jussieu, 75251 Paris Cedex 05, France.

10.1021/jp068323q CCC: $37.00
Published on Web 05/19/2007

provide a fit as good as the others and the obtained parameters were not physically acceptable. However, a modified hybrid model in which $e^-_{wb,1}$ does not relax and the relaxation of $e^-_{sb,2}$ assumes a change in position and shape of the spectrum, gives good results. From that analysis, we concluded that it was not obvious to select a unique model to depict the solvation dynamics of the electron in EG. We also deduced that the temporal behavior of the solvated electron in EG could be characterized by two time constants: a fast one of about 1−2 ps and a longer time around 25 ps. Moreover, we noticed a similarity between the picosecond time-resolved absorption spectrum of the electron in EG at room temperature and the absorption spectrum of the ground-state solvated electron recorded at higher temperature. That analogy would rather suggest a continuous relaxation.

To pursue and deepen that study, in this second paper, we investigate the formation of the solvated electron in both propanediols, propane-1,2-diol (12PD, propylene glycol) and propane-1,3-diol (13PD, trimethylene glycol). At room temperature, the macroscopic properties of those solvents are nearly the same. At 293 K, the dielectric constant ϵ is equal to 32 for 12PD and 35 for 13PD, the viscosity η is 49.5 and 49.3 cP, respectively. The values of the OH-group density are also very close (16.3×10^{21} and 16.7×10^{21} cm^{-3}, respectively). So the contribution of aliphatic and hydroxyl fragments on the solvation process can be studied, since 12PD bearing two vicinal OH groups can be regarded as an EG molecule with an additional methyl group and 13PD presents different separation of the hydroxyl groups. The optical absorption band of the solvated electron in the two propanediols is situated in the visible spectral domain with a maximum around 565 and 575 nm for 12PD and 13PD, respectively.[23−25] Recently, using nanosecond pulse radiolysis, we recorded the absorption spectra of the solvated electron in those solvents at different temperatures from 295 to 498 K.[24] In both solvents, the optical spectra shift to the red with increasing temperature. The temperature coefficient is more negative for 12PD than for 13PD and a change in the shape of the spectrum is noted only for 12PD. Those observations indicate larger modifications of the solvent structure and molecular interactions for 12PD than for 13PD, in agreement with the faster decrease in viscosity versus temperature for 12PD than for 13PD.

In the present study, time-resolved spectra were obtained for the electron produced by photoionization of the solvent with 263 nm femtosecond pulses. First, solvent ionization is checked to be due to a two-photon absorption process. and the two-photon absorption coefficient of both propanediols at 263 nm is determined. Then, the temporal evolution of transient absorption spectra of the electron is described and analyzed with several models using Bayesian data analysis method. Results for both propanediols are compared and discussed with reference to those previously obtained for EG.

2. Experimental and Data Analysis Methods

2.1. Experimental Section. The apparatus and procedures employed for the measurements reported here have already been described in detail in paper I. In short, the output of an amplified kilohertz femtosecond Ti:Sapphire laser system (Spectra Physics) was split into two parts to generate the pump and probe pulses. The pump beam at 263 nm was produced by frequency doubling and sum-frequency mixing in two BBO crystals of 90% of the fundamental beam. The pump beam was then focused on a 300 μm thick liquid jet in order to produce electrons by photoionization of the solvent. The pump beam diameter was usually set to 200 μm, while the pump pulse duration and energy was about 210 fs full width at half-maximum and 20 μJ, respectively. The remaining 10% of the fundamental beam at 790 nm was directed to a variable optical delay line and focused on a 3 mm sapphire disk to generate a white-light continuum. The continuum beam was divided into a probe and a reference beam by a broad band beam-splitter. The probe beam was focused onto the liquid jet sample. Then, the probe beam was dispersed on a polychromator and detected on a CCD camera (Princeton Instrument) with a resolution of 0.2 nm per pixel, simultaneously with the reference beam to take into account any laser fluctuations. Time-resolved spectra were recorded from 440 to 720 nm and corrected for the group velocity dispersion.

To study the dynamics of the electron, the transient absorbance signals were recorded in three temporal windows with different time resolutions. For the first temporal window and the best resolution, the delay time was increased up to 10 ps by steps of 100 fs and then to 50 ps by steps of 500 fs. These experiments, hereafter called "short-time" experiments, allowed us to resolve the beginning of the electron solvation. The "intermediate-time" experiments were associated to the temporal window of 100 ps with 45 steps of 250 fs followed by 90 steps of 1 ps. For the third temporal window with the lowest resolution, the delay time was increased up to 30−35 ps by steps of 1 ps and then to 470 ps by steps of 15 ps. These "long-time" experiments were used to evaluate the influence of the geminate recombination on the decay and the spectrum of the solvated electron. The transient absorption signals reported below were obtained using low peak power densities ($\leq$0.5 TW cm^{-2}), as in the case of EG, to be sure that the observed dynamics are independent of the electron concentration in our experimental conditions.

As depicted for EG in paper I, the transient absorption signals recorded at wavelengths below 600 nm, for both propanediols, exhibit a sharp "spike" at the time origin (the "coherent artifact") due to nonlinear absorption of the pump and probe light in the sample.[6,13,17,20]

For the nonlinear transmission experiments, the pump power density was changed by modifying the pump beam diameter on the sample moving the focusing lens and/or by varying the pump beam energy using a half-wave plate on the 790 nm beam. The incident and transmitted pump energy was measured just after the focusing lens and after the liquid jet, respectively.

Materials. Propane-1,2-diol from Aldrich (ACS Reagent) and propane-1,3-diol from Fluka (GC Grade) were used without further purification. The experiments were performed at room temperature (295 K).

2.2. Data Analysis. The complete description of our data analysis method, including data conditioning, Bayesian data analysis, and model selection, is given in paper I. However, we have improved the data conditioning in order to analyze simultaneously several experiments with different temporal windows. So the global analysis of the 2D spectro-kinetics data matrix **D** is performed to determine the kinetic and spectral parameters involved in the general expression for the transient absorbance:

$$D^{e}_{ij} \cong \sum_{k=1}^{n} c^{e}_{k}(t_i)\epsilon_k(t_i,\lambda_j) \qquad (1)$$

in the case of n absorbing species with molar extinction coefficient $\epsilon_k(t_i,\lambda_j)$ depending on time and wavelength and whose concentration $c^{e}_{k}(t_i)$ in experiment e is a function of time.

The "short-time" experiments over a 50 ps time window correspond to $N_t = 180$ points per wavelength, for "intermediate-time" experiments over 100 ps, $N_t = 135$, and for "long-time" experiments over 470 ps, $N_t = 65$. In the spectral domain, wavelengths between $\lambda = 440$ and 710 nm with a 10 nm step ($N_\lambda = 28$) have been considered. So the whole three experiments correspond to a total of $N_D = 10\,260$ data points to analyze, By truncating the "long-time" experiment to 100 ps to neglect the decay of the solvated electron due to geminate recombination, N_D is reduced to 8176.

The Bayesian probabilistic method is a powerful tool for data analysis, and its use allows us to deal with parameter optimization, parameter identification and model selection. The fit quality is assessed by the often used root-mean-square (rms):

$$\mathrm{rms} = \sqrt{\frac{1}{N_D}R^2} \tag{2}$$

and the Bayes information criterion (I_B), more reliable for comparison of models with different numbers of adjustable parameters:

$$I_B(M) = -0.5N_D \ln R^2 - 0.5N_\theta \ln N_D \tag{3}$$

where R^2 is the sum of squares of residuals between model and data, and N_θ is the number of optimized parameters. Better models are characterized by larger values of I_B, as the maximization of I_B is a competition between minimization of rms and minimization of the number of parameters.

3. Experimental Results

3.1. Two-Photon Absorption at 263 nm. As it is known that electrons generated in different photoprocesses have different thermalization and geminate recombination dynamics, it is important to identify whether the ionization of propanediols proceeds via a two- or three-photon excitation.[26] The ionization threshold of liquid 13PD is known to be 8.2 ± 0.1 eV.[27] To our knowledge, the ionization threshold of liquid 12PD has not been measured, but as the ionization threshold is found to be 8.3 ± 0.1 eV for both liquid EG and glycerol (propane-1,2,3-triol) and 8.2 ± 0.1 eV for liquid propan-1-ol,[27] we assume a similar value for 12PD. Consequently, the energy of 263 nm photons being 4.7 eV, the ionization of liquid propanediols should occur by a two-photon absorption mechanism.

The transmittance of the 300 μm liquid jet versus the peak power of the 263 nm input pulse is shown in Figure 1 for both propanediols. The observed evolution is characteristic of a single-beam two-photon absorption.[28−30] In that case, the measured transmittance (T) corresponding to the ratio of the transmitted pulse energy E to the incident pulse energy E_0 is given by

$$T = \frac{E}{E_0} = \frac{(1-R)^2}{E_0}\int_0^\infty \mathrm{d}r 2\pi r \int_{-\infty}^{\infty} \mathrm{d}t \frac{I_0(r,t)}{[1+\beta L(1-R)I_0(r,t)]} \tag{4}$$

where R represents the Fresnel reflection losses at the air−liquid jet interfaces and L is the jet thickness. We have fit our experimental values of the transmittance (T) as a function of the peak irradiance (I_0) with eq 4, and we have determined the values of β and R. We find that $\beta = (2.0 \pm 0.3) \times 10^{-11}$ m W^{-1} for 12PD and $\beta = (2.4 \pm 0.3) \times 10^{-11}$ m W^{-1} for 13PD while $R = 0.05$ for both propanediols (Figure 1). Those values of β are very similar to the value obtained in paper I for EG at 263 nm ($\beta = (2.1 \pm 0.1) \times 10^{-11}$ m W^{-1}) and also to the value found for water ($\beta = (1.8 \pm 0.1) \times 10^{-11}$ m W^{-1}) at 266 nm with 100 fs pulses.[30] But those values are 1 order of magnitude higher than the literature values obtained with picosecond laser pulses at 266 nm for water[28] and measured for other solvents at 264 nm with 200 fs pulses but on a lower intensity domain ($I_0 < 30$ GW cm^{-2}).[31] The obtained values of R are slightly larger than the values calculated with the refractive indexes (0.037 for 12PD, 0.038 for 13PD). The surface roughness of the jet inducing additional scattering can account for those differences.

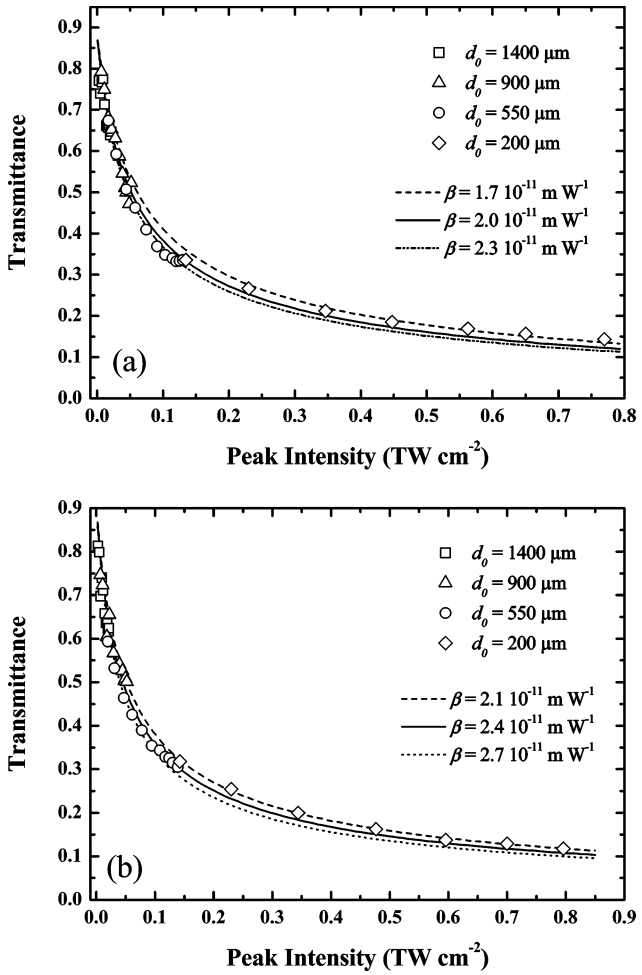

Figure 1. Transmittance of the 300 μm liquid jet versus the peak intensity of the 220 fs input pulse at 263 nm for (a) propane-1,2-diol and (b) propane-1,3-diol (symbol, experimental data for four different beam diameters; lines, calculated curves using eq 4 for different values of β and $R = 0.05$).

3.2. Formation of Solvated Electrons in Propanediols. Panels a and b of Figure 2 show the transient absorption kinetics recorded at three characteristic wavelengths (one in the blue part, one near the maximum and one in the red part of the absorption band of the solvated electron) upon photoionization of 12PD and 13PD, respectively. For each wavelength, three signals are presented corresponding to the three kinds of experiments performed with different temporal windows and steps (see section 2.1): "short-time" experiments over 50 ps, "intermediate-time" over 100 ps, and "long-time" over 470 ps. For clarity reasons, the signals are not corrected for the group velocity dispersion and plotted in logarithmic time scale. The main trends observed in these kinetics traces are similar for both propanediols. At zero-time delays between pump and probe pulses, the "coherent artifact" is visible for wavelengths below 580 nm. After the artifact, the signals at 440 nm slightly increase

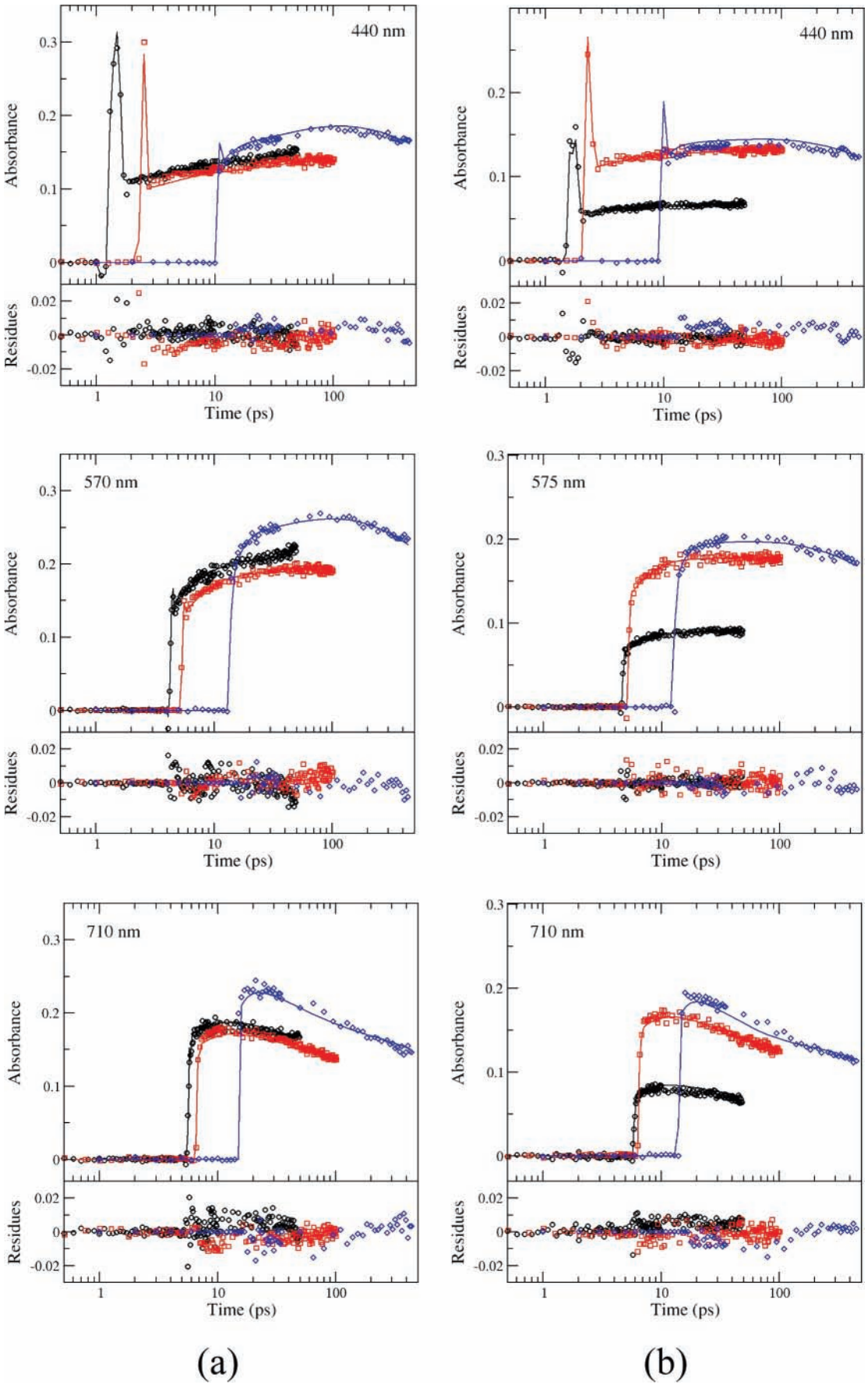

Figure 2. Transient absorption signals at three different wavelengths obtained upon 263 nm photoionization of (a) propane-1,2-diol and (b) propane-1,3-diol. For each wavelength, the kinetics signals originating from three experiments on different temporal windows (open symbols) are presented, and for clarity reasons, they are not corrected for the group velocity dispersion. The solid lines drawn through the points correspond to the best global fit obtained with the stepwise mechanism (STEP3P), and the fit residues are shown below.

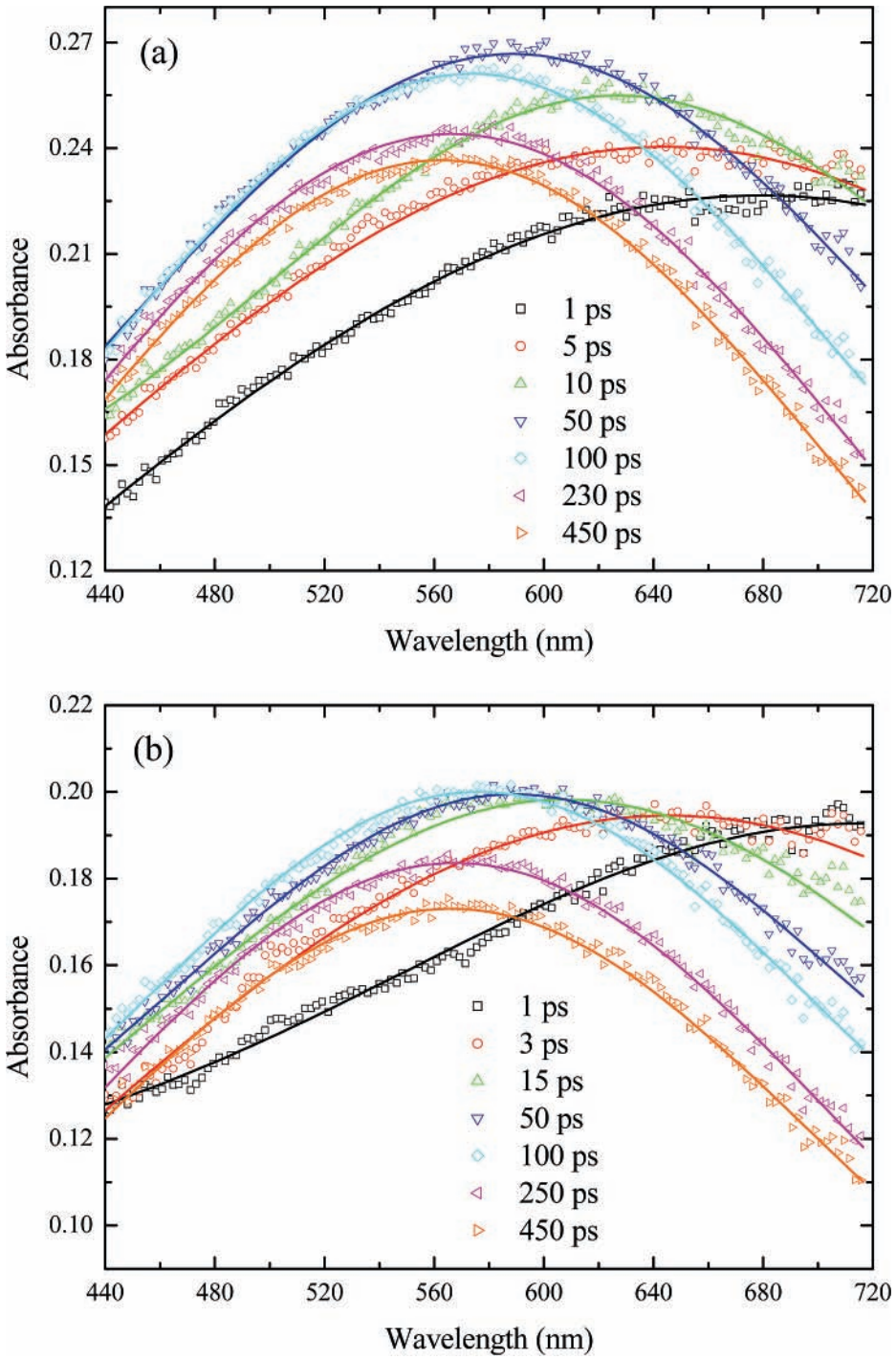

Figure 3. Time evolution of the absorption spectrum obtained in (a) propane-1,2-diol and (b) propane-1,3-diol upon two-photon ionization of the solvent at 263 nm. The solid lines through the points are just guides for the eyes.

for roughly 50 ps, and then, slowly decrease. The increase in the signals at 570−575 nm is more pronounced than at 440 nm and occurs mainly in the first 10 ps; the absorbance reaches a maximum around 50−100 ps and then decays. The signals at 710 nm rapidly increase during the pulse duration, remain quasi-constant for a few picoseconds and then, notably decrease for the next hundreds of picoseconds.

Panels a and b of Figure 3 show the time evolution over 450 ps of the absorption spectra measured in 12PD and 13PD, respectively, after photoionization of the solvent at 263 nm. The spectra are corrected for the group velocity dispersion and the first plotted spectra correspond to a time delay of 1 ps, consequently the "coherent artifact" around zero time delays is not present in the figures. For 12PD (Figure 3a), at early time ($t = 1$ ps), we observe a very broad absorption band with a maximum around 690 nm. As the blue part of this absorption band (below 650 nm) rises and the red part decreases, this band grows, narrows, shifts to shorter wavelengths, and reaches its highest amplitude around 50 ps with a maximum at 590 nm. Then, for the next 50 ps, the absorbance on the blue side ($\lambda <$ 540 nm) remains constant whereas the absorbance on the red side goes on decreasing. So the band becomes narrower, its amplitude slightly diminishes, and its maximum position continues to shift toward the blue spectral domain and almost reaches its equilibrium value at 100 ps. At longer time ($>$100 ps), the position and shape of the spectrum hardly change, but its intensity decays as the electron concentration diminishes due to geminate recombination.

The spectral evolution observed for 13PD (Figure 3b) looks like that for 12PD. During the first 15 ps, the red part of the absorbance rapidly drops while the blue part rises, inducing a shrinkage and a blue shift of the broad initial absorption band. So, the position of the band is around 720 nm at 1 ps and 610 nm at 15 ps. Afterward, the red side of the spectrum continues to slowly decrease and the blue side to increase, and the absorption spectrum of the fully solvated electron with its maximum at 575 nm is obtained around 100 ps. The subsequent global decrease of the spectrum is due to geminate recombination. We remark that the main difference between both solvents is that, during the solvation process for the first 100 ps, the intensity of the shifting spectrum of the excess electron remains quasi-constant for 13PD while it increases for 12PD.

4. Data Analysis and Discussion

4.1. Models for Solvation Dynamics. Up to now, many models of electron solvation and relaxation, at all levels of theory, have been suggested,[1,5,14,16,32−36] to explain all the experimental results. In paper I on the solvation dynamics of the electron in EG, we found it worthwhile to analyze our data with various approaches, and in total, we tested 11 models based on sequential stepwise mechanisms and continuous relaxation processes. Four models gave a good quality fit of our spectro-kinetics signals with a minimum number of adjustable parameters: a two-step model (STEP3), a heterogeneous (CRELH) or biexponential (CREX2) continuous relaxation model, and a modified hybrid model with a stepwise transition followed by a homogeneous continuous relaxation (HYBM). Taking into account those results, for the present study, we have retained the first three models, the simplest ones. All the details of the models are given in paper I and resumed hereafter.

As in paper I, for all the models, the "coherent artifact" around the zero time delay is described by a time-symmetric combination of three generalized Gaussian functions:

$$\begin{aligned} A_0(t,E) = &-a_1(E)\mathcal{G}(t;t_0(E)-\Delta,\gamma_1,\alpha) \\ &+ a_2(E)\mathcal{G}(t;t_0(E),\gamma_2,\alpha) \\ &- a_3(E)\mathcal{G}(t;t_0(E)+\Delta,\gamma_1,\alpha) \end{aligned} \quad (5)$$

with:

$$\mathcal{G}(t;\, t_0,\, \gamma,\, \alpha) = \exp\left(-\left|\frac{t-t_0}{\gamma}\right|^{\alpha}\right) \quad (6)$$

and $\alpha \geq 2$, and where $t_0(E)$ corresponds to the group velocity dispersion curve in energy space.

For the sequential stepwise relaxation cascades, inasmuch as three species were necessary but sufficient to accurately fit the data of the electron in EG, only the two-step mechanism with three species (STEP3P) has been considered to account for the electron solvation in both propanediols. Each considered species or states of the electron is supposed to have a fixed and individual spectrum. The time-dependent absorbance is then written:

$$A(t,E) = A_0(t,E) + \mathcal{G}(t;t_0(E),\sigma/\sqrt{4\ln 2},2) \otimes \sum_{k=1}^{3} c_k(t)\epsilon_k(E) \quad (7)$$

where $\mathcal{G}(t;t_0(E),\sigma/\sqrt{4\ln 2},2)$ represents the instrumental response function (cross correlation of the pump and probe pulses) and the $\otimes$ symbol stands for the convolution operator. The concentration curves $c_k(t)$ are obtained analytically by the standard Laplace transform method and spectra have been modeled by a lognormal shape function S:

$$\epsilon_k(E) = \epsilon_k S(E;E_{\max,k},\Omega_k,\gamma_k) \quad (8)$$

where S is parametrized by the peak position $E_{\max}$, the full width at half-maximum Ω, and the asymmetry factor γ (see Appendix).

Models of continuous spectral evolution where the time-dependent absorption spectrum of a unique species is described by a lognormal function with time-dependent coefficients have also been tested:

$$\begin{aligned} A(t,E) = A_0(t,E) + \mathcal{G}(t;t_0(E),\sigma/\sqrt{4\ln 2},2) \otimes \\ [c_0\epsilon(t) \times S(E;E_{\max}(t),\Omega(t),\gamma(t))] \end{aligned} \quad (9)$$

To account for the presence of various solvation sites and/or relaxation rates heterogeneity, the time-dependence of each parameter ($x = \epsilon,\ E_{\max},\ \Omega,\ \gamma$) is modeled either by a biexponential function (CREX2):

$$x(t) = x_\infty + \Delta_{x,1}\mathcal{G}(t;0,\tau_{x,1},1) + \Delta_{x,2}\mathcal{G}(t;0,\tau_{x,2},1) \quad (10)$$

or by a specific stretched exponential function (CRELH):

$$x(t) = x_\infty + \Delta_x\mathcal{G}(t;0,\tau_x,\beta_x); \qquad 0 < \beta_x \leq 1 \quad (11)$$

In that latter case, two characteristic times can be defined for each parameter x in terms of the gamma function Γ: the average relaxation time given by $\langle\tau_x\rangle = \tau_x\beta_x^{-1}\Gamma(\beta_x^{-1})$, and the average lifetime $\langle t_x\rangle = \tau_x\Gamma(2\beta_x^{-1})/\Gamma(\beta_x^{-1})$.

4.2. Data Analysis. Geminate recombination of the electron is neglected in our analysis; consequently, unless it is otherwise stated, the spectro-kinetics data in both propanediols were truncated to the time-window of 100 ps. Indeed, according to previous work on these solvants,[25] any decay of the solvated electron is observed at picosecond time range till 200 ps, and, from the time-resolved spectra shown in Figure 3, geminate recombination appears unimportant. So in our models, the solvated electron as the final species can be considered to be stable and have an infinite lifetime. However, at 100 ps, the spectral evolution is not fully achieved and the spectrum of the solvated electron was explicitly introduced in the models. The parameters of the spectra (Table 2) have been obtained by fitting the absorption spectra of the solvated electron obtained by nanosecond pulse radiolysis experiments.[24,25] We checked that those spectral parameters correspond to the transient photolysis spectra measured at $t > 450$ ps, indicating that the solvation process is completed at that delay time.

4.2.1. Stepwise Modeling. The retained three-state model (STEP3P) provides good fit of our experimental data for both propanediols (Table 1 and Figure 2). The optimal spectra and kinetics of the three species are displayed in Figure 4, and the values of the parameters are reported in Table 3.

According to this model (Figure 4a,b and Table 3), the weakly bound electron, e^-_{wb}, converts into the intermediate species, e^-_{sb}, with a time constant τ_1 of about 4.5 ps for 12PD and 3 ps for 13PD. The strongly bound, e^-_{sb} gives much slowly the solvated electron, e^-_s, with a time constant τ_2 around 54.6 and 34.6 ps for 12PD and 13PD, respectively. The values of τ_1 and τ_2 obtained for both propanediols are higher than those obtained for EG (1.3 and 25 ps) in paper I. That can be explained by the much higher viscosity and the slightly lower dielectric constant of the propanediols ($\eta \cong 49.5$ and $\epsilon \cong 32-35$) compared to

TABLE 1: Comparison between the Different Parametric Models Used to Fit the Experimental Data on the Solvation of Electron in Propanediols

solvent	model name	scheme	comments	N_θ[a]	rms (10^{-3})[b]	I_B[c]
12PD	STEP3P	$e^-_{wb} \longrightarrow e^-_{sb} \longrightarrow e^-_s$	two-step process	10	4.45	7409
	CREX2	$e^-_{wb} \longrightarrow e^-_s$	biexponential relaxation	12	4.12	8010
	CRELH	$e^-_{wb} \longrightarrow e^-_s$	heterogeneous relaxation	10	4.39	7517
13PD	STEP3P	$e^-_{wb} \longrightarrow e^-_{sb} \longrightarrow e^-_s$	two-step process	10	3.24	10332
	CREX2	$e^-_{wb} \longrightarrow e^-_s$	biexponential relaxation	12	3.15	10575
	CRELH	$e^-_{wb} \longrightarrow e^-_s$	heterogeneous relaxation	10	3.18	10490

[a] Number of adjusted parameters excluding "coherent artifact". [b] Root-mean-square. [c] Bayes Information criterion.

TABLE 2: Parameters of the Lognormal Functions Used to Fit the Absorption Spectra of the Solvated Electron Obtained by Nanosecond Pulse Radiolysis in Propanediols

solvent	ϵ (M^{-1} cm^{-1})	$E_{max,}$ (eV)	Ω (eV)	γ
12PD	9700	2.192 ± 0.005	1.489 ± 0.012	1.82 ± 0.03
13PD	10000	2.176 ± 0.006	1.574 ± 0.017	2.00 ± 0.04

EG ($\eta = 16$, $\epsilon = 38$). These values are reasonable in reference to the times determined in other alcohols,[6,16] particularly, for the series of linear alcohols (methanol, ethanol, butanol).[6] Nevertheless, we remark that both times, τ_1 and τ_2, are longer for 12PD than for 13 PD despite their similar macroscopic properties.

The absorption spectra of the three species involved in the STEP3P model are shown in Figure 4c for 12PD and 4d for 13PD. The first species (e^-_{wb}) which appears after solvent ionization, presents a structureless absorption in the visible domain with an absorption maximum in the IR domain. Being located outside of the observation window, the position of the absorption maximum for the initially generated electron e^-_{wb} is crudely determined. The second species (e^-_{sb}) shows a quite broad absorption band in the visible domain with a maximum around 630 nm for both propanediols. This band is close to that of the fully solvated electron e^-_s, highlighting the quick formation of well-localized electrons and suggesting the presence of pre-existing traps in the solvent.

It is to be noted that, if geminate recombination is crudely approximated by a first-order process, we may adjust the "long-time" signals up to 470 ps with a third time constant around 1.9 ns (Figure 2). That result indicates that the disappearance of the solvated electron is very slow and confirms that the geminate recombination could be neglected over 100 ps.

4.2.2. Continuous Relaxation Modeling. In our analysis, the "continuous shift" model has been improved since, not only the position but also the shape of the absorption spectrum of the electron may change during the solvation process. Indeed, the experimental transient absorption spectra (Figure 3) were fitted to lognormal curves and the optimized parameters ϵ, E_{max}, Ω, and γ are plotted as a function of time in Figure 5. From the plots, for both propanediols, we note that the increase in the extinction coefficient ϵ is faster than the increase in the band energy E_{max} or the decrease in the bandwidth Ω. ϵ reaches its equilibrium value (Table 2) in about 20 ps while E_{max} and Ω still evolve. The values of the asymmetry factor γ are quite dispersed and not well-defined, especially at short time, because the transient absorption spectra exhibit a very broad absorption band in the visible but also the near-infrared domain, out of our experimental spectral window.

We performed a fit of our spectro-kinetics data considering a time-dependent absorption spectrum of a unique species. First, the time dependence of the spectral parameters was described by biexponential functions (CREX2). Values of the parameters are reported in Table 4. The kinetics of ϵ appeared to be monoexponential with a time constant τ_ϵ of 5.6 and 2.9 ps for 12PD and 13PD, respectively. These time values are close to those found for τ_1 (4.5 and 3.2 ps for 12PD and 13PD, respectively) with STEP3P. As γ cannot be accurately determined at short times due to our experimental spectral window, the shorter time was undefined and a single-exponential evolution was retained, leading to a characteristic time τ_γ of 19.8 and 13.6 ps for 12PD and 13PD, respectively. In contrast to paper I for EG, unconstrained adjustments did not lead to similar characteristic times for E_{max} and Ω. We checked that, if the characteristic times were constrained to be the same for E_{max}, Ω, and γ, as in paper I for EG, the fit quality was poor, so such constrains could not be justified. For 12PD, the values of the characteristic times are found to be $\tau_{Emax1} \cong 0.65$ ps, $\tau_{Emax2} \cong 27.5$ ps, $\tau_{\Omega 1} \cong 1$ ps, and $\tau_{\Omega 2} \cong 76$ ps. The first characteristic times are small and quite close in regard to our experimental resolution, while the second times are almost 2 orders of magnitude higher and differ from each other by nearly a factor 3. Although they are in the same range, they also differ from the value of τ_2 (54.6 ps) determined with STEP3P. For 13PD, the time constant values found with CREX2 are: $\tau_{Emax1} \cong 0.25$ ps, $\tau_{Emax2} \cong 20.5$ ps, $\tau_{\Omega 1} \cong 2.6$ ps, and $\tau_{\Omega 2} \cong 40.5$ ps. The very short time obtained for E_{max} ($\tau_{Emax1} \cong 0.25$ ps) is not actually reliable considering the pulse duration and the signal around time zero due to nonlinear effects; such a fast component might be an analysis artifact resulting from our way to model the "coherent artifact" which interferes with the measurement till 0.5 ps. The value obtained for $\tau_{\Omega 1}$ is in the neighborhood of those already mentioned for τ_ϵ (CREX2) and τ_1 (STEP3P). The τ_{Emax2} and $\tau_{\Omega 2}$ values are of the same order of magnitude and lie on either side of the τ_2 value determined with STEP3P. As in the case of EG in paper I, for both solvents and parameters, the average lifetimes are dominated by the long time components; the values of $\langle\tau_{Emax}\rangle$ and $\langle\tau_\Omega\rangle$ are 25.3 and 72.5 ps for 12PD and 19.6 and 39.0 ps for 13PD, respectively. So whatever the parameters, the average lifetime $\langle\tau_x\rangle$ is longer for 12PD than 13PD corroborating the fact that the solvation process is faster in 13PD than in 12PD.

Second, we considered stretched exponential type decays for the spectral parameters (CRELH). Such functions are often used to describe the non-exponential behavior of complex dynamics found in liquids or glasses, mostly due to disorder inherent in soft condensed matter.[37] Values of the parameters are reported in Table 5. As for CREX2, the peak intensity ϵ and the asymmetry factor γ appear to have single-exponential dynamics for both propanediols. In contrast, E_{max} and Ω present strong heterogeneous behaviors as $\beta_x < 0.5$ leading to very different values for the characteristic relaxation time τ_x and the average times $\langle\tau_x\rangle$ and $\langle t_x\rangle$. Indeed, values of β_x as small as 0.12 relate to an overall τ-distribution of very broad width, and in such case, it is to be wondered what is the physical meaning of the

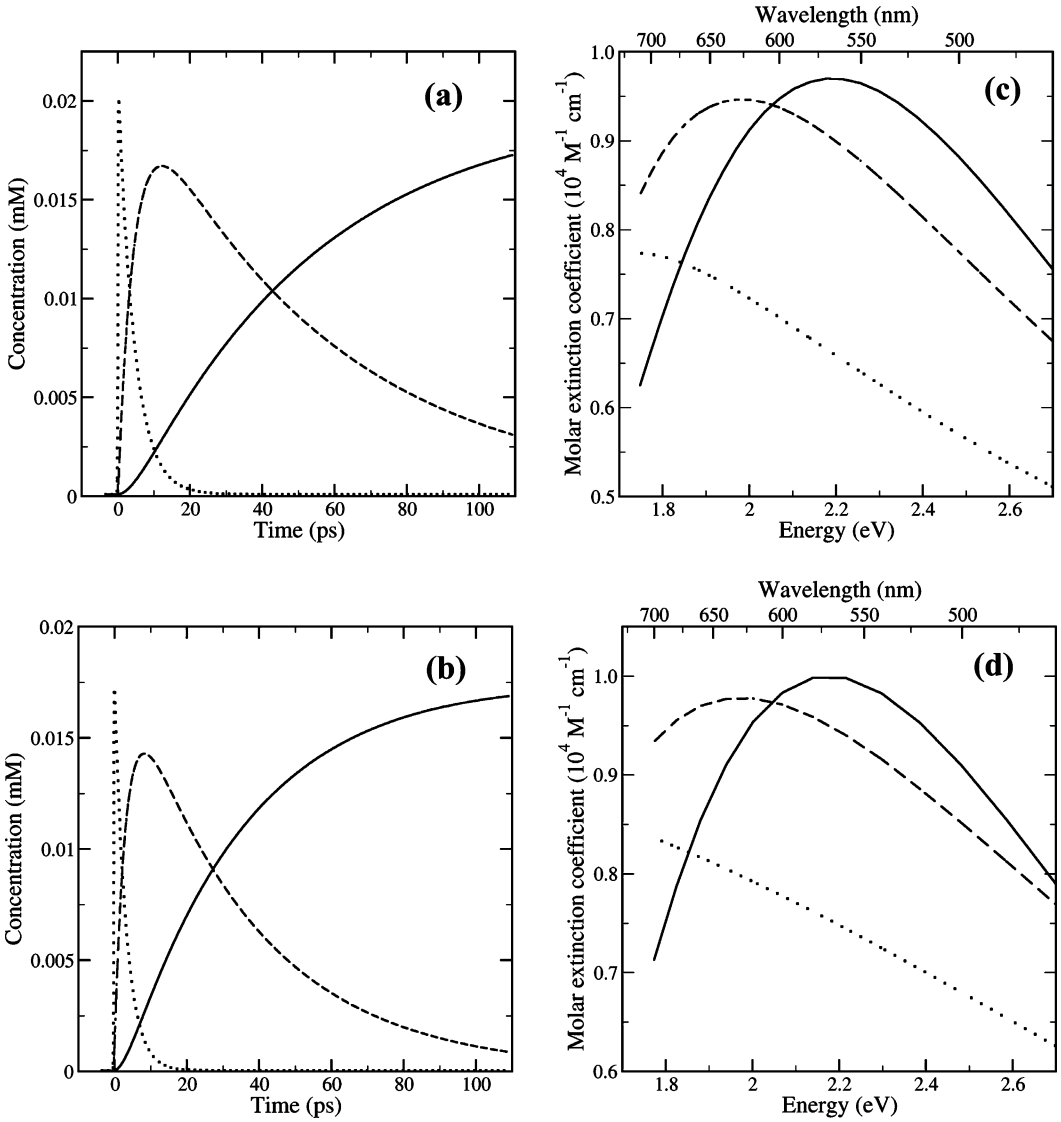

Figure 4. (a, b) Time evolution of the concentrations and (c, d) absorption spectra of the three species involved in the stepwise mechanism (STEP3P) used to fit the experimental data in (a, c) propane-1,2-diol and (b, d) propane-1,3-diol: (•••) e_{wb}^-, (- - -) e_{sb}^-, and (—) e_s^-.

TABLE 3: Parameters of STEP3P Model Resulting from the Probabilistic Analysis of the Experimental Data for the Solvation of Electron in Propanediols

solvent		e_{wb}^-	e_{sb}^-	e_s^-
12PD	ϵ (M^{-1} cm^{-1})	7570 ± 100	9350 ± 100	9700
	E_{max} (eV)	1.70 ± 0.05	1.97 ± 0.03	2.192
	Ω (eV)	1.9 ± 0.1	1.7 ± 0.1	1.489
	γ	6 ± 1	2.9 ± 0.1	1.82
	τ (ps)	4.5 ± 0.1	54.6 ± 0.5	
13PD	ϵ (M^{-1} cm^{-1})	8850 ± 200	9780 ± 100	10 000
	E_{max} (eV)	1.3 ± 0.1	2.0 ± 0.1	2.176
	Ω (eV)	3.3 ± 0.2	2.1 ± 0.1	1.574
	γ	2.2 ± 0.4	3.1 ± 0.4	2.00
	τ (ps)	3.2 ± 0.1	34.6 ± 0.7	

deduced times. The problem could arise from the fact that the derivative of the stretched exponential diverges as $t \rightarrow 0$ inducing the presence of very short times which need to be balanced by much longer components. However, despite a difficult physical interpretation of the function, we note that the time evolution of the spectral parameters obtained with CRELH resembles that determined with CREX2 (Figure 5). As expected from the previous remark, the main differences occur at short times for E_{max} and Ω, but also for the parameter γ which is not so well-defined experimentally.

4.3. Discussion. If we compare the results of the Bayesian analysis of our spectro-kinetics data with the different parametric models (Table 1), we find that the three models, STEP3P, CREX2 and CRELH, provide acceptable fits (rms ≤ 4.5×10^{-3}). But, as the number of adjustable parameters is not identical for the three models, the Bayesian criterion, I_B, confirms that the best fit of our data for both propanediols is obtained with CREX2.

In paper I concerning the electron solvation in EG, the best adjustment of the transient absorption signals was also per-

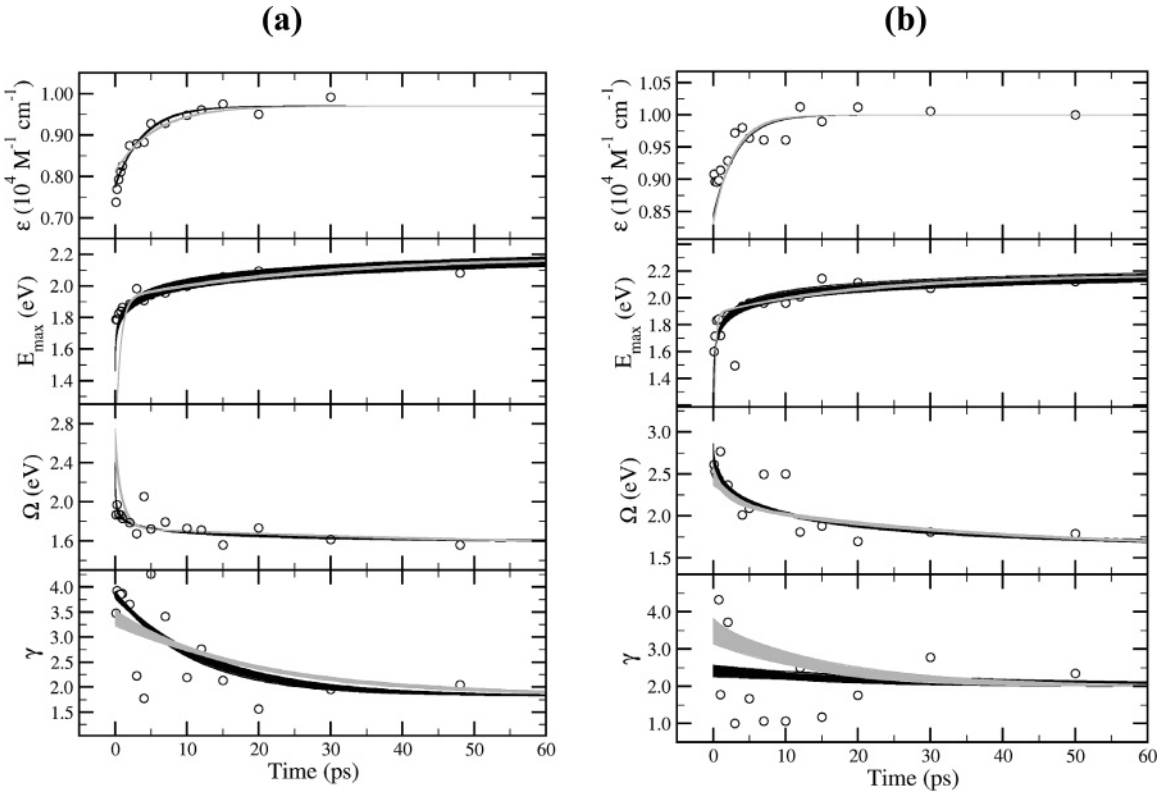

Figure 5. Time evolution of the spectral parameters, ϵ, the molar extinction coefficient, E_{max}, the peak position, Ω, the full-width at half-maximum, and γ the asymmetry factor obtained by fitting individually each experimental transient spectra with a lognormal function (open circles) or by fitting the full spectro-kinetics data with a biexponential (gray lines, CREX2) or a heterogeneous continuous relaxation model (black lines, CRELH) in (a) propane-1,2-diol and (b) propane-1,3-diol.

TABLE 4: Parameters of CREX2 Model Resulting from the Probabilistic Analysis of the Experimental Data for the Solvation of Electron in Propanediols

solvent	x	x_∞	Δ_{x1}	τ_{x1} (ps)	Δ_{x2}	τ_{x2} (ps)	$\langle\tau_x\rangle$ (ps)
12PD	ϵ	9700 M^{-1} cm^{-1}	-1570 ± 10 M^{-1} cm^{-1}	5.64 ± 0.09			5.6
	E_{max}	2.192 eV	-1.02 ± 0.04 eV	0.65 ± 0.02	-0.27 ± 0.01 eV	27.5 ± 0.7	25.3
	Ω	1.489 eV	0.88 ± 0.08 eV	0.97 ± 0.08	0.24 ± 0.01 eV	75.9 ± 3.5	72.5
	γ	1.82	1.56 ± 0.06	19.8 ± 1.0			19.8
13PD	ϵ	10 000 M^{-1} cm^{-1}	-1665 ± 15 M^{-1} cm^{-1}	2.88 ± 0.04			
	E_{max}	2.176 eV	-1.29 ± 0.09 eV	0.24 ± 0.02	-0.29 ± 0.01 eV	20.6 ± 0.7	19.6
	Ω	1.574 eV	0.35 ± 0.03 eV	2.6 ± 0.6	0.55 ± 0.02	40.5 ± 1.4	39.0
	γ	2.00	1.5 ± 0.1	13.6 ± 1.6			

TABLE 5: Parameters of CRELH Model Resulting from the Probabilistic Analysis of the Experimental Data for the Solvation of Electron in Propanediols

solvent	x	x_∞	Δ_x	τ_x (ps)	β_x	$\langle\tau_x\rangle$ (ps)	$\langle t_x\rangle$ (ps)
12PD	ϵ	9700 M^{-1} cm^{-1}	-1925 ± 15 M^{-1} cm^{-1}	3.91 ± 0.05	1	3.9	3.9
	E_{max}	2.192 eV	-0.98 ± 0.01 eV	6.1 ± 1.1	0.24 ± 0.01	188	8165
	Ω	1.489 eV	1.92 ± 0.05 eV	0.010 ± 0.001	0.12 ± 0.01	828	8×10^6
	γ	1.82	2.02 ± 0.03	12.2 ± 0.7	1	12.2	12.2
13PD	ϵ	10 000 M^{-1} cm^{-1}	-1605 ± 20 M^{-1} cm^{-1}	3.07 ± 0.06	1	3.0	3.0
	E_{max}	2.176 eV	-2.14 ± 0.03 eV	0.11 ± 0.01	0.16 ± 0.01	121	73 830
	Ω	1.574 eV	1.21 ± 0.05 eV	10.1 ± 0.9	0.46 ± 0.02	24	88
	γ	2.00 eV	0.42 ± 0.08	29.0 ± 1.0	1	29.0	29.0

formed with CREX2. However, in that solvent, the two time constants determined with CREX2 for the time-dependent spectral parameters were found to be the same ($\tau_{Emax1} \cong \tau_{\Omega 1} \cong \tau_{\gamma 1} \cong 1.7$ ps and $\tau_{Emax2} \cong \tau_{\Omega 2} \cong \tau_{\gamma 2} \cong 25.5$ ps) and close to the lifetimes of the intermediate species determined with STEP3P model ($\tau_1 \cong 1.3$ ps, $\tau_2 \cong 25.0$ ps). So it was possible to extract two characteristic times for the electron solvation dynamics in EG: a short time of about 1−2 ps, and a longer one around 25 ps. In the present study for 12PD and 13PD, it is not so easy to deduce the relevant times, since the time constants obtained in CREX2 for the time-dependent parameters are not similar and differ from the values of the lifetimes in STEP3P.

It has been suggested that electron solvation characteristic times could be related to relaxation times derived by permittivity measurements, either the dielectric relaxation time, τ_{D2},[38] or the longitudinal relaxation time $\tau_{L1} = \tau_{D1}\epsilon_{\infty 1}/\epsilon_{01}$.[2] τ_{D1} corresponds to the cooperative relaxation time of hydrogen bonded alcohol network and τ_{L1} accounts for the presence of an excess charge, while τ_{D2} refers to the reorientation time of the alcohol monomer; ϵ_{0i} and $\epsilon_{\infty i}$ are the permittivity relaxation parameters

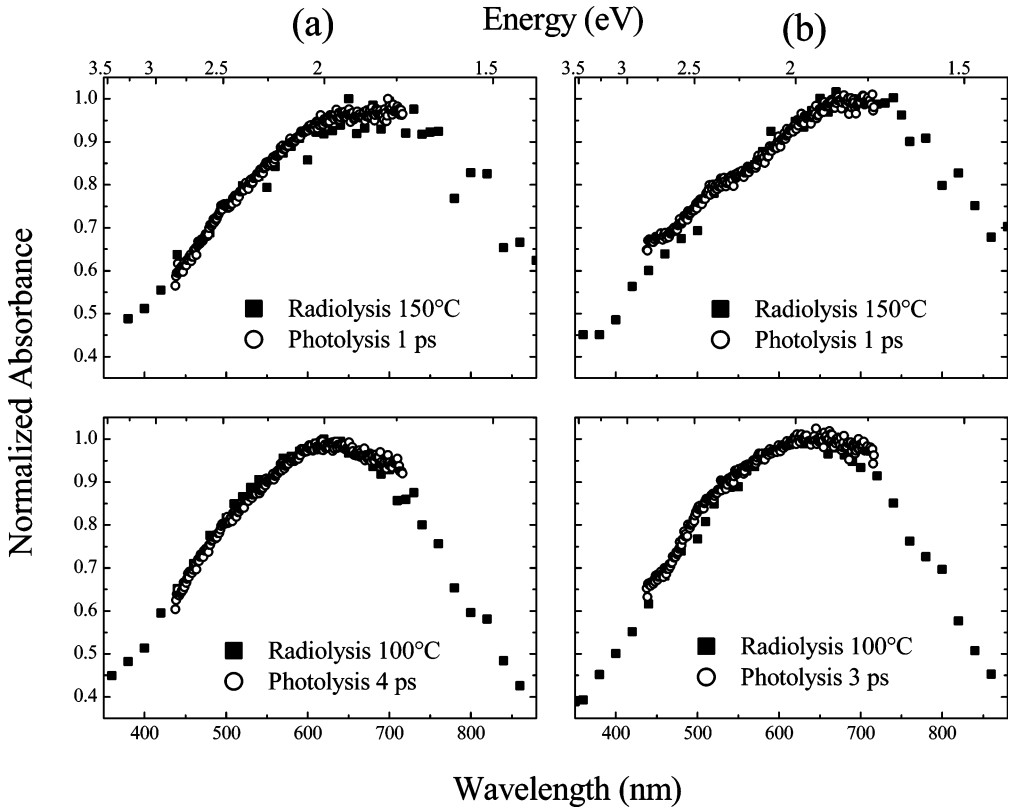

Figure 6. Comparison between the absorption spectra recorded at early time after photoionization at 263 nm (○) and the absorption spectra of the solvated electron obtained at high temperature by pulse radiolysis (■) (taken from ref 24) in (a) propane-1,2-diol and (b) propane-1,3-diol.

known from the Argand diagram for each relaxation process. For 12PD, Barthel and Buchner performed permittivity measurements at microwave to far-infrared frequencies.[39] Considering Debye-type (exponential) relaxation processes, they reported values of 430 and 40 ps for τ_{D1} and $\tau_{D2,}$ respectively, with $\epsilon = \epsilon_{01} = 29.2$, $\epsilon_{\infty 1} = \epsilon_{02} = 5.9$ and $\epsilon_{\infty 2} = \epsilon_{03} = 3.9$, which leads to 86.9 and 26.4 ps for τ_{L1} and τ_{L2}, respectively.[39] So we may note a correlation between our estimations of the long solvation times with CREX2 ($\tau_{E\max 2} \cong 27.5$ ps and $\tau_{\Omega 2} \cong 76$ ps) and the values of τ_{L2} and τ_{L1}, respectively. Dielectric spectra (up to 72 GHz) were also measured by Becker and Stockhausen for 12PD and 13PD.[40] They analyzed the spectra into a sum of four Debye components characterized by relaxation times τ_i with $i = 1-4$ and found values around 450, 200, 25, and 3 ps for 12PD and 450, 200, 35, and 6 ps for 13PD. We remark that, for 12PD, the relaxation time τ_1 is close to the τ_{D1} value of Barthel and Buchner but the second relaxation times differ significantly. In that case, it is rather the τ_3 value (25 and 35 ps for 12PD and 13PD, respectively) which is close to one of our solvation times, $\tau_{E\max 2} \cong 27.5$ ps for 12PD, and $\tau_{\Omega 2} \cong 40.5$ ps for 13PD. Other dielectric relaxation studies have been performed with 13PD, but in order to account for the shape of the measured spectra, different relaxation terms have been used in the spectral function. For instance, Wang et al. described their permittivity data with a Debye term for the low-frequency part and a Cole−Cole term for the highest part and obtained $\tau_D = 340$ ps and $\tau_{cc} = 35$ ps for the Debye and Cole−Cole relaxation times, respectively.[41] In the study of Hanna et al., the relaxation spectra were analyzed in a single Cole-Davidson term and an effective relaxation time $\beta\tau_1$ of 398 ps was obtained with a Cole-Davidson distribution parameter β of 0.88.[42] As for Sudo and co-workers, they used the stretched exponential function (Kolhrausch−Williams−Watts function) to fit the frequency dependence of the complex permittivity and they determined the relaxation time τ and the asymmetrical broadness parameter β_K of the relaxation curve to be ~300 ps and 0.945, respectively.[43] It is worth noticing that β_K is slightly lower than 1, indicating a small asymmetric broadening of the dielectric loss interpreted by weak heterogeneities in the size and dynamical structure of cooperative domains in the liquid, and that the value of τ ranges between τ_{D1} and τ_{D2} found by Becker and Stockhausen.[40] Those results of dielectric measurements differ significantly from our values of β_x and τ_x obtained for E_{max} and Ω with CRELH. Indeed, the small values of β_{Emax} and β_Ω are related to very broad distributions of relaxation times suggesting great heterogeneities in the spatial and dynamical structure of the solvent. As already mentioned in paper I, dielectric and electron solvation measurements seem to probe different solvent responses. Consequently, the relations between solvation experiments and dielectric measurements are not straightforward, all the more so since the time values deduced in both cases greatly depend on the chosen models.

For the two studied propanediols, the best adjustments of the data are obtained with the continuous relaxation models, CREX2 and also CRELH. Further evidence for the continuous character of the solvation process is given in Figure 6 by the time−temperature analogy. Such an analogy was also noticed in paper I for EG, and had already been made for water.[14,44] The transient spectra recorded at room temperature after the photoionization at 1 and 4 ps for 12PD (Figure 6a), and 1 and 3 ps for 13PD (Figure 6b) are similar to the spectra of the solvated electron in the equilibrated state at higher temperatures, 150 and 100 °C, respectively.[24] That similarity between spectra tends to indicate a comparable organization disorder of the solvent (increasing with T or as t tends to 0). Since the solvation process appears as a continuous process in our experimental conditions, that suggests that the photogenerated electrons are rapidly trapped, with a characteristic time shorter than our temporal resolution

and that the observed electrons are only localized electrons, what agrees with a reported electron trapping of less than 1 ps for alcohols at room temperature.[11] Moreover, we observe a "faster cooling" for the trapped electrons in 13PD compared to 12PD, in agreement with the solvation times obtained shorter in 13PD than in 12PD and the fact that the solvent macroscopic properties, such as viscosity, are more affected by an increase in temperature for 12PD than for 13PD.

Slower electron solvation dynamics in 12PD than in 13PD and EG had already been reported by Okazaki et al., but at 215 K, not at room temperature.[23] Okazaki et al. reported that for all the diols at $T \geq 240$ K, the spectra reached their equilibrium shape within the 150 ns after the start of the 100 ns radiation pulse and then decayed uniformly at all energies, indicating that the electrons had relaxed to the equilibrium solvated state within the time resolution of the measurement. However, at 215 K, in 12PD, the optical spectrum of the electron shifted unsymmetrically toward higher energy for the first 500 ns. By approximating the decay of the low-energy side and the growth of the high-energy side of the band as first order, they estimated a mean decay time of 160 ns and a mean growth time of 40 ns at 215 K.[23] Those results corroborate our observations of a change in the shape of the electron spectrum during the solvation. Time evolution of the spectral shape has also been observed for the electron produced in D_2O by multiphoton ionization[20] and, lately, for the electron generated by above the gap (12.4 eV) two-photon ionization of liquid H_2O and D_2O.[17] In both studies, a Gaussian−Lorentzian analysis of the transient absorption spectra was performed and gave evidence for a decrease in the Gaussian width with time. To interpret these observations,[20] Pépin et al. extended their "hybrid model", previously used to explain the electron solvation in methanol,[5] by adding an unknown species that absorbs in the near-infrared (800−1100 nm). In their hybrid model, two unrelaxed trapped electrons, $e^-_{wb,1}$ and $e^-_{sb,2}$ undergo continuous blue shift with the same characteristic time; concurrently $e^-_{wb,1}$ transforms into $e^-_{sb,2}$, which relaxes to the solvated electron. In the model, the absorption spectrum of each species remains constant in shape and amplitude, only the energy changes. In the work of Lian and co-workers,[17] two regimes of the spectral evolution of the presolvated electron in light and heavy water were observed. For both of these regimes, the spectral profile changes considerably with time. In the first picosecond after photoionization, new spectral features (1.15 μm band and 1.4 μm shoulder for H_2O, 1.4 μm peak for D_2O) were detected in the near-infrared domain where O−H and O−D overtones appear in the spectrum of liquid water. At later delay time ($t >$ 1 ps), the position of the band maximum is "locked", but the spectral profile continues to change. Vibronic coupling, vibrational relaxation in the water molecules lining the solvation cavity, and time-dependent decrease in the size and sphericity of the solvation cavity were suggested as possible causes for the observed spectral transformations. Our experimental results on solvation dynamics of electron in both propanediols and in ethylene glycol show very similar behaviors: in particular, the spectral profiles of excess electrons change during solvation. Therefore, we can consider that similar explanations might apply to our observations of the evolution of the absorption spectra of electrons in polyols. Indeed, from the theory of the absorption spectrum of the excess electron they developed,[45−48] Abramczyk and co-workers had already pointed out that the coupling between the excess electron and the intramolecular modes of the solvent plays the dominant role on the absorption bands of the excess electron both in the visible and near-IR, and that the dynamics of the solvated electron is mainly governed by the vibrational properties of matrices in which the electron is trapped. Moreover, their theoretical model has led to the conclusion that two kinds of trapped electrons exist in alcohols: visible absorbing electrons associated with the hydroxyl traps (coupling with the bending mode C−OH) and IR-absorbing electrons trapped in the alkyl group (coupling with the CH stretching modes).[47] This model has been recently supported by the resonance Raman experiments performed by Tauber and Mathies.[49−51] Their resonance Raman experiments provided valuable data on the ground state vibrational structure and excited-state nuclear dynamics of the hydrated electron, corroborating the cavity model with water molecules directly hydrogen-bonded to the electron.[50] Resonance Raman spectra in primary alcohols (methanol, ethanol, propan-1-ol) also revealed strong vibronic coupling of the solvated electron to at least five normal modes of the solvent.[51] The spectra showed enhancements of the downshifted OH stretch, the OH in-plane bend and the OH out-of-plane bend (torsion), which were analogous to the enhanced modes of the aqueous solvated electron. In addition, Franck−Condon coupling of the electronic excitation to methyl/methylene deformations demonstrated that the electronic wave function of the solvated electron extended significantly into the alkyl group of the alcohols.[51] The possible participation of C−H interactions in stabilizing the solvated electron had already been suggested by ab initio calculations of methanol clusters anions.[52] Contributions of alkyl groups may be understood from the geometrical structure of the solvated electron in ethanol[53,54] and ethylene glycol[55] glasses determined from electron spin echo modulation experiments performed by Narayana and Kevan. From their analyses, they deduced that, in ethanol, four first-solvation shell molecules were arranged tetrahedrally around the electron with a molecular dipole orientation, i.e., with the bisector of the COH bond angle approximately oriented toward the electron.[53,54] For the solvated electron in ethylene glycol, they also suggested a total of four first solvation shell molecules but with only two of these having their OH groups oriented toward the electron.[55] The existence of two kinds of traps, respectively where the paraffinic and the hydroxyl groups are locally concentrated, had been evidenced at 77 K only for monohydroxy-alcohols and not for polyhydroxy-alcohols, indicating that, in the latter solvents, the phase is not segregated into polar and nonpolar regions owing to the abundance of the H-bonds.[56] Consequently, we believe that the time evolution of the spectral profiles of excess electrons we observed in propanediols and ethylene glycol is not due to a conversion from an electron mainly trapped by alkyl groups to an electron mainly trapped by hydroxyl groups but is related to vibronic coupling and vibrational relaxation in the first-solvation shell molecules, concomitant with conformational rearrangements. To get a better insight into the electron solvation in diols, we initiated theoretical investigations and molecular simulations are in progress.

5. Conclusion

We followed the formation of solvated electron in neat propanediols using pump−probe transient absorption spectroscopy in the visible spectral range from 440 to 710 nm. The electrons were generated with a 263 nm femtosecond laser pulse by the photoionization of the solvent according to a two-photon absorption process. The two-photon absorption coefficient at 263 nm was estimated to be $\beta = (2.0 \pm 0.3) \times 10^{-11}$ for 12PD and $(2.4 \pm 0.3) \times 10^{-11}$ m/W for 13PD. The excess electron in both propanediols presents a wide absorption band in the visible

and the near-IR at very short delay time after the pump pulse. The time-resolved spectra revealed that a localized electron which absorbs in the blue spectral domain is quickly formed and relaxes to the equilibrated solvated electron in a couple of tens picosecond. That spectral evolution appears faster for 13PD than 12PD.

Using Bayesian data analysis method, we performed a fitting procedure of the spectro-kinetics signals with three solvation models: a two-step mechanism, a biexponential or heterogeneous continuous relaxation model. The three models were able to adjust correctly the data for both propanediols, indicating that it is not obvious to select a solvation model. Nevertheless, the best fits were obtained by the biexponential continuous relaxation model. But as the time constants are different for all the spectral parameters, it is difficult to extract the main solvation characteristic times. However, the values of the time constants were found to be shorter for 13PD than 12PD, confirming the faster solvation process in 13PD compared to 12PD. Moreover, the analogy between the time evolution of the solvated electron absorption spectrum at room temperature and the temperature dependence of the absorption spectrum of the equilibrated solvated electron gives further evidence of the continuous character of the solvation process: the spectral evolution in time is mostly caused by the continuous relaxation of the electron trapped in a large distribution of solvent cages. It is worth noticing that the slower solvation dynamics corresponds to the vicinal diol, 12PD, suggesting greater molecular changes in close proximity of the electron site which have longer range effects. For instance, that may indicate a different number of first solvation shell molecules, insofar as only one or both of the OH groups of the diol molecule may be involved in the electron cavity. Hence, molecular simulations are under way to elucidate the structures and rearrangements of the solvent molecules responsible for the solvation of the electron.

6. Appendix

In this study, absorption spectra have been modeled by 3-parameter lognormal functions (peak position E_{max}, full width at half-maximum Ω and asymmetry factor γ):

$$S(E;E_{max},\Omega,\gamma) = u^{-1}\exp\left(-\frac{1}{2}(\sigma^2 + \ln^2(u)/\sigma^2)\right) \quad (12)$$

where the auxiliary parameters are defined by

$$\sigma = \ln(\gamma)/2\sqrt{2} \quad (13)$$

$$u = (E - \vartheta)/m \quad (14)$$

$$m = \Omega/[2\exp(-\sigma^2)\sinh(\ln\gamma)] \quad (15)$$

and

$$\vartheta = E_{max} - m\exp(-\sigma^2) \quad (16)$$

The normalization is chosen such that the maximal value is $S(E_{max};E_{max},\Omega,\gamma) = 1$; accordingly, the peak area is

$$I_S = \sqrt{2\pi}m\sigma\exp(-\sigma^2/2) \quad (17)$$

References and Notes

(1) Migus, A.; Gauduel, Y.; Martin, J. L.; Antonetti, A. *Phys. Rev. Lett.* **1987**, *58*, 1559.
(2) Hirata, Y.; Mataga, N. *J. Phys. Chem.* **1990**, *94*, 8503.
(3) Long, F. H.; Lu, H.; Eisenthal, K. B. *Phys. Rev. Lett.* **1990**, *64*, 1469.
(4) Sander, M.; Brummund, U.; Luther, K.; Troe, J. *Ber. Bunsen-Ges. Phys. Chem.* **1992**, *96*, 1486.
(5) Pépin, C.; Goulet, T.; Houde, D.; Jay-Gerin, J.-P. *J. Phys. Chem.* **1994**, *98*, 7009.
(6) Shi, X.; Long, F. H.; Lu, H.; Eisenthal, K. B. *J. Phys. Chem.* **1995**, *99*, 6917.
(7) Turi, L.; Holpar, P.; Keszei, E. *J. Phys. Chem. A* **1997**, *101*, 5469.
(8) Silva, C.; Walhout, P. K.; Reid, P. J.; Barbara, P. F. *J. Phys. Chem. A* **1998**, *102*, 5701.
(9) Silva, C.; Walhout, P. K.; Yokoyama, K.; Barbara, P. F. *Phys. Rev. Lett.* **1998**, *80*, 1086.
(10) Emde, M. F.; Baltuska, A.; Kummrow, A.; Pshenichnikov, M. S.; Wiersma, D. A. *Phys. Rev. Lett.* **1998**, *80*, 4645.
(11) Goulet, T.; Pépin, C.; Houde, D.; Jay-Gerin, J.-P. *Radiat. Phys. Chem.* **1999**, *54*, 441.
(12) Assel, M.; Laenen, R.; Laubereau, A. *J. Chem. Phys.* **1999**, *111*, 6869.
(13) Hertwig, A.; Hippler, H.; Unterreiner, A.-N. *Phys. Chem. Chem. Phys.* **1999**, *1*, 5633.
(14) Madsen, D.; Thomsen, C. L.; Thogersen, J.; Keiding, S. R. *J. Chem. Phys.* **2000**, *113*, 1126.
(15) Kloepfer, J. A.; Vilchiz, V. H.; Lenchenkov, V. A.; Germaine, A. C.; Bradforth, S. E. *J. Chem. Phys.* **2000**, *113*, 6288.
(16) Scheidt, T.; Laenen, R. *Chem. Phys. Lett.* **2003**, *371*, 445.
(17) Lian, R.; Crowell, R. A.; Shkrob, I. A. *J. Phys. Chem. A* **2005**, *109*, 1510.
(18) Thaller, A.; Laenen, R.; Laubereau, A. *J. Chem. Phys.* **2006**, *124*, 024515.
(19) Vilchiz, V. H.; Kloepfer, J. A.; Germaine, A. C.; Lenchenkov, V. A.; Bradforth, S. E. *J. Phys. Chem. A* **2001**, *105*, 1711.
(20) Pépin, C.; Goulet, T.; Houde, D.; Jay-Gerin, J.-P. *J. Phys. Chem. A* **1997**, *101*, 4351.
(21) Holpar, P.; Megyes, T.; Keszei, E. *Radiat. Phys. Chem.* **1999**, *55*, 573.
(22) Soroushian, B.; Lampre, I.; Bonin, J.; Pernot, P.; Pommeret, S.; Mostafavi, M. *J. Phys. Chem. A* **2006**, *110*, 1705.
(23) Okazaki, K.; Idriss-Ali, K. M.; Freeman, G. R. *Can. J. Chem.* **1984**, *62*, 2223.
(24) Lampre, I.; Lin, M.; He, H.; Han, Z.; Mostafavi, M.; Katsumura, Y. *Chem. Phys. Lett.* **2005**, *402*, 192.
(25) Lin, M.; Mostafavi, M.; Muroya, Y.; Han, Z.; Lampre, I.; Katsumura, Y. *J. Phys. Chem. A* **2006**, *110*, 11404.
(26) Crowell, R. A.; Bartels, D. M. *J. Phys. Chem.* **1996**, *100*, 17940.
(27) Jung, J.-M. *Research Habilitation Report*; University Louis Pasteur: Strasbourg I, France, 2003.
(28) Nikogosyan, D. N.; Oraevsky, A. A.; Rupasov, V. I. *Chem. Phys.* **1983**, *77*, 131.
(29) Reuther, A.; Laubereau, A.; Nikogosyan, D. N. *J. Phys. Chem.* **1996**, *100*, 16794.
(30) Pommeret, S.; Gobert, F.; Mostafavi, M.; Lampre, I.; Mialocq, J.-C. *J. Phys. Chem. A* **2001**, *105*, 11400.
(31) Dragomir, A.; McInerney, J. G.; Nikogosyan, D. N.; Ruth, A. A. *IEEE J. Quantum Electron.* **2002**, *38*, 31.
(32) Fueki, K.; Feng, D.-F.; Kevan, L. *J. Phys. Chem.* **1974**, *78*.
(33) Rossky, P. J.; Schnitker, J. *J. Phys. Chem.* **1988**, *92*, 4277.
(34) Keszei, E.; Murphrey, T. H.; Rossky, P. J. *J. Phys. Chem.* **1995**, *99*, 22.
(35) Bratos, S.; Leickman, J.-C. *Chem. Phys. Lett.* **1996**, *261*, 117.
(36) Zharikov, A. A.; Fisher, S. F. *J. Chem. Phys.* **2006**, *124*, 054506.
(37) Richert, R. *J. Phys. Condens. Matter* **2002**, *14*, R703.
(38) Chase, W. J.; Hunt, J. W. *J. Phys. Chem.* **1975**, *79*, 2835.
(39) Barthel, J.; Buchner, R. *Pure Appl. Chem.* **1991**, *63*, 1473.
(40) Becker, U.; Stockhausen, M. *J. Molec. Liq.* **1999**, *81*, 89.
(41) Wang, F.; Pottel, R.; Kaatze, U. *J. Phys. Chem. B* **1997**, *101*, 922.
(42) Hanna, F. F.; Gestblom, B.; Soliman, A. *Phys. Chem. Chem. Phys.* **2000**, *2*, 5071.
(43) Sudo, S.; Shinyashiki, N.; Kitsuki, Y.; Yagihara, S. *J. Phys. Chem. A* **2002**, *106*, 458.
(44) Crowell, R. A.; Lian, R.; Shkrob, I. A.; Qian, J.; Oulianov, D. A.; Pommeret, S. *J. Phys. Chem. A* **2004**, *108*, 9105.
(45) Abramczyk, H. *J. Phys. Chem.* **1991**, *95*, 6149.
(46) Abramczyk, H.; Kroh, J. *J. Phys. Chem.* **1991**, *95*, 6155.
(47) Abramczyk, H.; Kroh, J. *Radiat. Phys. Chem.* **1992**, *39*, 99.
(48) Abramczyk, H.; Kroh, J. *Radiat. Phys. Chem.* **1994**, *43*, 291.
(49) Tauber, M. J.; Mathies, R. A. *Chem. Phys. Lett.* **2002**, *354*, 518.
(50) Tauber, M. J.; Mathies, R. A. *J. Am. Chem. Soc.* **2003**, *125*, 1394.
(51) Tauber, M. J.; Stuart, C. M.; Mathies, R. A. *J. Am. Chem. Soc.* **2004**, *126*, 3414.
(52) Turi, L. *J. Chem. Phys.* **1999**, *110*, 10364.
(53) Narayana, M.; Kevan, L. *J. Chem. Phys.* **1980**, *72*, 2891.
(54) Narayana, M.; Kevan, L. *J. Am. Chem. Soc.* **1981**, *103*, 1618.
(55) Narayana, M.; Kevan, L.; Samskog, P. O.; Lund, A.; Kispert, L. D. *J. Chem. Phys.* **1984**, *81*, 2297.
(56) Shida, T.; Iwata, S.; Watanabe, T. *J. Phys. Chem.* **1972**, *76*, 3683.